UNIVERSIDADE FEDERAL DO CEARÁ
CENTRO DE TECNOLOGIA
DEPARTAMENTO DE ENGENHARIA HIDRÁULICA E AMBIENTAL
PROGRAMA DE PÓS-GRADUAÇÃO EM RECURSOS HÍDRICOS

RENATO QUINDERÉ CARNEIRO

PALEOCLIMATIC DROUGHT: RAINFALL VARIABILITY ANALYSIS

FORTALEZA

2021

RENATO QUINDERÉ CARNEIRO

PALEOCLIMATIC DROUGHT: RAINFALL VARIABILITY ANALYSIS

Dissertação apresentada ao Programa de Pós-Graduação em Recursos Hídricos e Saneamento Ambiental da Universidade Federal do Ceará, como requisito parcial à obtenção do título de Mestre em Engenharia Civil. Área de concentração: Recursos Hídricos.

Orientador: Prof. Dr. Francisco de Assis de Souza Filho

FORTALEZA

2021

Dados Internacionais de Catalogação na Publicação
Universidade Federal do Ceará
Biblioteca Universitária
Gerada automaticamente pelo módulo Catalog, mediante os dados fornecidos pelo(a) autor(a)

C29p Carneiro, Renato Quinderé.
Paleoclimatic Drought: Rainfall Variability Analysis / Renato Quinderé Carneiro. – 2021.
48 f. : il. color.

Dissertação (mestrado) – Universidade Federal do Ceará, Centro de Tecnologia, Programa de Pós-Graduação em Engenharia Civil: Recursos Hídricos, Fortaleza, 2021.
Orientação: Prof. Dr. Francisco de Assis de Souza Filho.

1. Last Millennium. 2. Model Comparison. 3. Oscillatory Modes. I. Título.

CDD 627

RENATO QUINDERÉ CARNEIRO

PALEOCLIMATIC DROUGHT: RAINFALL VARIABILITY ANALYSIS

Dissertação apresentada ao Programa de Pós-Graduação em Recursos Hídricos e Saneamento Ambiental da Universidade Federal do Ceará, como requisito parcial à obtenção do título de Mestre em Engenharia Civil. Área de concentração: Recursos Hídricos.

Aprovada em: 15/04/2021

BANCA EXAMINADORA

Prof. Dr. Francisco de Assis de Souza Filho (Orientador)

Universidade Federal do Ceará (UFC)

Prof. Dr. Eduardo Sávio Passos Rodrigues Martins

Universidade Federal do Ceará (UFC)

Prof. Dr. Alexandre Araújo Costa

Universidade Federal do Ceará (UECE)

AGRADECIMENTOS

À Deus.

Aos meus pais, a quem devo tudo.

A minha esposa, cujo incentivo e apoio tornaram possíveis a minha participação no programa e a conclusão deste trabalho.

Aos meus irmãos, que me encorajaram a enfrentar este desafio.

Aos professores do DEHA, em especial ao professor Assis, por sua inestimável orientação nos últimos dois anos.

Aos colegas da CAIXA, que me incentivaram a buscar novos conhecimentos.

Aos colegas do programa, com quem compartilhei essa jornada.

" Pluralitas non est ponenda sine neccesitate."

William of Ockham

RESUMO

O conhecimento da variabilidade climática é fundamental na atividade de planejamento no âmbito dos Recursos Hídricos. Esse conhecimento, no entanto, pode levar a conclusões equivocadas quando fundamentado em séries provenientes de observações, isto porque essas séries normalmente não são longas o suficiente para representar a variabilidade do clima em toda a sua amplitude. A reconstrução do clima por meio de variável *proxy* tem tido muito sucesso em obter séries mais longas, mas encontra dificuldades em regiões tropicais como o Nordeste Brasileiro. A abordagem adotada neste estudo é utilizar resultados de modelos paleoclimáticos provenientes do experimento do Ultimo Milênio do PMIP para avaliar a variabilidade do clima. Para tanto, é necessário avaliar a capacidade do modelo em representar o clima da região estudada. A primeira parte deste estudo propõe um método de avaliação de modelos que decompõe as séries em componentes sazonais e plurianuais e compara o resultado com as séries observadas por meio de medidas da Teoria da Informação. A hierarquização dos modelos foi realizada utilizando-se o TOPSIS em três cenários diferentes. Na segunda parte, os modelos mais bem classificados para o cenário de variabilidade plurianual foram avaliados por meio do teste CUSUM livre de distribuição e da análise *Wavelet* com intuito de detectar *change points* e modos oscilatórios. Os modelos também foram comparados entre si e com as forçantes solar e vulcânica para avaliar se os modos detectados se deviam à variabilidade interna do sistema ou à forçantes externas. A comparação de modelos no cenário de sazonalidade mostrou que CSIRO-Mk3L-1-2, bcc-csm1-1 e CCSM4 foram os modelos com melhor aderência à série observada, enquanto que a comparação no cenário plurianual mostrou que HadCM3, MPI-ESM -P e EC-Earth3-Veg-LR foram os modelos com melhor aderência. No terceiro cenário, o melhor desempenho ficou por conta dos modelos bcc-csm1-1, MRI-ESM2-0 e HadCM3. Na segunda parte, nenhum *change point* foi detectado nos modelos a um nível de confiança de 95%, ao passo que a Análise *Wavelet* detectou modos oscilatórios com períodos variando de 4 a 8 anos, 16 a 32 anos e 128 a 256 anos. Comparações entre modelos e as séries de forçantes externas levaram a evidências de que o modo de variação com um período de 128 a 256 anos pode ser decorrente de forçantes externas.

Palavras-Chave: Último Milênio, Comparação de Modelos, Modos Oscilatórios

ABSTRACT

Climate variability knowledge is key information in water resources planning. This information, however, could be misleading if based only on observed series since these usually are not long enough to represent the variability in its full range. Climate reconstitution by a proxy variable is very successful in extending these series, but it finds difficulties when dealing with tropical regions such as NEB. The approach adopted in this study is to use Paleoclimatic model output from PMIP´s last millennium experiment to assess Climate variability, which leads to the problem of assessing the model´s ability to represent the climate of the studied region. In its first part, this study proposes a method for model evaluation which decomposes the series in seasonal and pluriannual components and compares the result to observed series using measures from Information Theory. The model ranking was obtained by TOPSIS in three different scenarios. In the second part, the top-ranked models for the pluriannual variability scenario were assessed through the distribution-free CUSUM test and Wavelet analysis to detect change points and oscillatory modes. Models were also compared to each other and to both solar irradiation and volcanic forcing to assess whether the detected modes were due to internal variability or to external forcings. Model comparison simulations in the seasonality scenario showed that CSIRO-Mk3L-1-2, bcc-csm1-1, and CCSM4 were the models with the best adherence to the observed series, while simulations in the pluriannual scenario showed that HadCM3, MPI-ESM-P, and EC-Earth3-Veg-LR were the models with the best adherence. In the third scenario, the best performance was due to models bcc-csm1-1, MRI-ESM2-0, and HadCM3. In the second part, no change point was detected in the series with a confidence level of 95%., while in Wavelet Analysis modes with a period range of 4 to 8 years, 16 to 32 years, and 128 to 256 years were detected. Comparisons between models and external forcings analysis led to evidence that the mode with a period range of 128 to 256 years could be caused by external forcings.

Keywords: Last Millennium, Model Comparison, Oscillatory Modes

LIST OF FIGURES

LIST OF TABLES

LIST OF ABBREVIATIONS AND ACRONYMS

CEEMD	Complete Ensemble Empirical Mode Decomposition
CUSUM	Cumulative Sum
EEMD	Ensemble Empirical Mode Decomposition
EMD	Empirical Mode Decomposition
ENSO	El Niño-Southern Oscillation
FUNCEME	Fundação Cearense de Meteorologia e Recursos Hídricos
IMF	Intrinsic Mode Functions
KL Divergence	Kullback-Liebler Divergence
LM	Last Millennium
MD	Mutual Information Diagram
NEB	Brazilian Northeast Region
PMIP	Paleoclimatic Modeling Intercomparison Project
TOPSIS	Technique for Order of Preference by Similarity to Ideal Solution
VI	Variation of Information

SUMMARY

1 INTRODUCTION

Extreme hydrological events cause damages to humankind every year with consequences that include human life losses and huge economic damage, with impacts that overcome the ones due to other natural hazards as earthquakes and volcanoes. Beyond these direct destructive effects, devastating secondary effects such as starvation, fire and epidemics usually follow from these events. In terms of economic losses, these events have a yearly cost of several billions of dollars, even in developed nations. Despite the technological progress and investments in both structural and non-structural measures to mitigate this hazard, many regions are still vulnerable to these events (Kundzewicz et al., 1993).

Among the extreme hydrological events, droughts are natural hazards that occur in most countries and are not limited to dry regions. Although there is no consensus on its precise definition, drought could be understood as cumulative rainfall deficit. As opposed to other natural hazards, which usually have immediate effects, drought´s consequences may take some time to appear as reduced stream flow or low reservoir levels, and hence it is difficult to determine precisely both its starting point and end. Characterized by non-structural damages spread through a large geographic area, it affects more people than any other natural hazard (World Meteorological Organization, 2006).

Brazilian Northeast Region (NEB) is characterized mostly by semiarid conditions with an annual rainfall average ranging from 400 to 800 mm and evaporation levels as high as 3000 mm. Associated with the precipitation seasonal regime, which usually occurs from February to May, the shallow crystalline soil results in intermittent rivers, especially in the northern area. This region, which by its natural characteristics is vulnerable to droughts, has suffered from frequent severe droughts with documented records that date back to the 16th century. As a response to this hazard, the Brazilian Government invested heavily in hydraulic infrastructure, represented mainly by reservoir construction, with public policies evolving through time from the Hydraulic Paradigm to Sustainable Development and Integrated Water Resource Management, besides financial aids and relief programs (Campos, 2015).

Despite the government efforts to mitigate droughts effects, the drought persistence over several years could still stress the hydraulic infrastructure. As an instance, a report by Martins & Magalhães (2015) on the situation of the current drought event, which started in 2012, indicates that in September 2013 almost 50% of the reservoirs had storage levels lower than 10%. As for larger reservoirs, the historical series shows that the current event caused the Castanhão Reservoir to reach storage levels as low as 10% after a dry period

of 4 years and reached its minimum storage of 2,1% in 2018. Martins & Magalhães (2015) also reported the drought´s effects such as livestock death, crop failure and population migratory movements, many of which resemble the impacts of secular droughts events.

The infrastructure investment may have changed the hydraulic potential of the region, raising the environmental limit (Campos, 2015) and leading the system to a different equilibrium state, but the system is still constrained by the region´s rainfall regime. Additionally, as stated by Woodhouse & Overpeck (1998) climatic low-frequency variability patterns can be associated with an enhanced likelihood of persistent drought events. This way, it is imperative to understand climate variability patterns in order to design policies that deal properly with pluriannual droughts.

Climate variability patterns could occur in time scales that range from seasonal to centennial and are caused by both system´s internally generated variability and external forcings. While Internally generated variability results of the dynamical process operating within the atmosphere and the interactions between the atmosphere and other components of the earth system, the externally forced variability could be enforced, among others, by solar irradiation, volcanic aerosol, and atmospheric composition (Wallace & Hobbs, 2006).

Assessing low-frequency patterns from observed series could lead to false conclusions as these series might not be representative of the climate variability amplitude due to the series limited length, as the evidence gathered by Woodhouse & Overpeck (1998). For instance, Woodhouse & Overpeck (1998) concluded, based on paleoclimatic data, that droughts that occurred in the 21st century across the United States are not representative of the full range of possible variations on climate conditions of today. As in this study, paleoclimatic data is widely used to reconstruct the past climate and could extend the observed series to overcome this issue. Among the proxy variables adopted for climate reconstruction, Woodhouse & Overpeck (1998) mentions tree-ring, lake sediment, alluvial, eolian and archaeological sources.

Another approach is to assess climate variability through paleoclimatic models, which is more adequate to NEB since paleoclimatic data is almost unavailable for this region. Climate models are climate system´s numerical representations computed from physical laws and are the primary source for climate assessments (Gregory Flato et al., 2018) with paleoclimatic experiments simulating the past climate. The Last Millennium experiment, from Paleoclimate Modeling Intercomparison Project (PMIP), simulates the climate from the year 850 to 1849, which had climate conditions similar to the present and, hence, is suited to assess natural climate variability and the distinction between internally generated variability and

externally forced variability (Jungclaus et al., 2017). In this context, Mann et al. (2021) assessed the Atlantic Multidecadal Oscillation forcings through an ensemble of climate models and concluded that the volcanic forcing was the major influence on this variation mode during the last millennium with no evidence that it was internally generated by the Climate system.

This dissertation assesses rainfall low-frequency variation patterns through paleoclimatic models and is organized in the following parts: objectives, article entitled Paleoclimatic Drought: Rainfall Variability Analysis, conclusions, references and appendix.

2 OBJECTIVE

2.1 Main Objective

The main objective of this study is to assess rainfall variability through the analysis of paleoclimatic models output in order to detect low-frequency oscillatory modes with periodicity ranging from decadal to centennial scales.

2.2 Specific Objectives

- Evaluate models capacity to represent climate in Brazilian Northeast Region.
- Rank climate models according their adherence to observed series.
- Identify the significant low-frequency oscillatory modes represented in climate models for the period from the year 850 to 1849, and correlate these modes to solar and volcanic forcings.

3 PALEOCLIMATIC DROUGHT: RAINFALL VARIABILITY ANALYSIS

3.1 Introduction

Climate variability plays a key role in water resources planning. A better understanding of climate variability would help policymakers and managers to improve the investment allocation on climate adaptation (National Academies of Sciences and Medicine, 2016).

Woodhouse et al. (2016) suggested that is not possible to understand the climate variability from rainfall/stream flow gauge series. The main issue addressed is that such series are not long enough, usually, they are about 100 years long, so the variability represented in these series usually have lower amplitude than the climate variability, an issue also mentioned by Milly et al. (2008) and Miller et al. (2018).

One way to overcome this problem is to estimate longer series by proxy variables, as it was accomplished by several dendrochronology studies (e.g. Martin et al., 2019; Malevich et al., 2013; Cook et al., 2013;Woodhouse et al., 2011). This method, however, seems to struggle against some difficulties when applied to tropical dry regions such as NEB, in a way that this kind of information is unavailable for this region (Roberto, Aragão, Groenendijk, & Sergio, 2019; Wils et al., 2010; Worbes & Nin, 2002).

Viana et al. (2014) studied another proxy variable and inferred the Boqueirão Lake water level, in Brazilian northeast, for the last 2.000 years based on sediment analysis. Despite this successful application, this method still faces the challenge of regionalization, since, according to Gomes et al. (2014), Brazilian lake density is low and few lakes in Brazil are deep enough to accommodate long settling time.

Another approach is to assess climate variability through climate model´s outputs, which is widely used. This approach, however, leads to the problem of assessing the model´s ability to represent the climate of the studied region (Gregory Flato et al., 2018). Several studies assess climate models performance, particularly in NEB, Dias et al. (2019) compared models to investigate whether they were capable of reproducing climate patterns in that region. This study calculates the climatological mean for the annual cycle and adopts Pearson´s correlation associated with the mean squared error as a metric and, additionally, analyses qualitatively the annual mean rainfall spatial pattern. Likewise, Almagro et al. (2020), after downscaling, evaluates models performance in Brazil through metrics such as Pearson´s correlation and mean squared error applied to long term climatological mean, which

is similar to the procedure adopted by both Worku et al (2018) and Samadi et al. (2010) applied to different countries.

The use of measures that require the model´s output and observations to be paired, such as Pearson´s correlation and RMSE, enforces researchers to limit the analysis to compare point estimates, such as long term means. This restriction is usually due to the fact reported by Gregory Flato et al. (2018) that there is no guarantee that models and observation are in the same phase in respect of internal variation modes. As a consequence, comparisons are not assessing the underlying probability distribution and may lead to deceptive conclusions. In order to overcome this issue, Thorarinsdottir et al. (2013) assess measures to compare the model´s output probability distribution to the empirical probability distribution obtained through gauged series. A list of desirable properties is analyzed for these measures and the proper ones are listed, among which the authors highlight the Kullback-Liebler Divergence (KL Divergence).

The aim of this study is to assess climate variability through the analysis of paleoclimatic models output in order to detect low-frequency oscillatory modes with periodicity ranging from decadal to centennial scales. The hypothesis is that longer series provided by paleoclimatic models could embed low-frequency oscillatory modes that are impossible to detect in observed series due to their limited length. In order to achieve this objective, a method for climate model selection based on measures from information theory, such as KL Divergence, is proposed. This method is then applied to models from Paleoclimate Modeling Intercomparison Project (PMIP) phase 3 and 4 to evaluate the adherence to the NEB. After that, the models with the best representation of NEB´s rainfall pluriannual variability were analyzed focusing on variation modes from decadal to centennial scales.

3.2 Methods

3.2.1 Dataset

The rainfall data used were provided by the PMIP for NEB, and it is accessible to download at https://esgf-node.llnl.gov/search/cmip6/. The PMIP is an initiative that, in order to understand climate change mechanisms, coordinates climate modeling activities and model evaluation.

Last Millennium (LM) is part of the PMIP set of simulations. It allows evaluating the performance of climate models constrained by reconstructed forcings (volcanic, solar

irradiance, greenhouse gases etc) and investigating both the response of the climate to these forcings during that period and climate variability in longer time scales than usually assessed by century-long simulations, e.g., the traditional historical simulation (Taylor, 2012). Those external forcings are described in detail by Schmidt et al. (2011, 2012). It is generally acknowledged that there might be significant uncertainties, especially regarding volcanic forcing, but either way PMIP models show an adequate response, within the range of uncertainty from early observations and reconstructions of climate variables such as temperature (Masson-Delmotte, 2013).

The LM experiment includes the period from the year 850 to 1850 and is suited to study climate natural variability in a state that is close to that of the present-day (Braconnot et al., 2012). This period is well documented with historical records and proxy variables and is useful to investigate the distinction between the climate variability due to the system´s internal modes from the variability caused by external forcings. The LM experiments were included in both PMIP phases 3 and 4, and considered climate forcing such as orbital parameters changes, greenhouse gas concentrations, solar irradiance, and stratospheric aerosols of volcanic origin. Additionally, LM simulations were complemented by historical simulations comprising the period from 1850 to the present day (Jungclaus et al., 2017).

This study contains models for which there is available precipitation output for the Last Millennium experiment from PMIP phases 3 and 4. Table 1 indicates the models that fulfilled this requirement, which were 9 models from 8 institutes. The historical dataset for these models were compared to the gauged series obtained from Fundação Cearense de Meteorologia e Recursos Hídricos (FUNCEME) in order to determine which model is more adherent to the NEB. Since the models and the gauged series cover different time span, the period of analysis was from 1911 to 2005, which is covered for all of them.

Table 1 - Models included in this analysis

#	Phase	Model Name	Institution
1	PMIP 3	bcc-csm1-1	Beijing Climate Centre System Model
2	PMIP 3	CCSM4	Community Climate System Model
3	PMIP 3	CSIRO-Mk3L-1-2	Common wealth Science and Industrial Research Organization
4	PMIP 3	HadCM3	Hadley Centre for Climate Prediction and Research
5	PMIP 3	MPI-ESM-P	Max Plank Institute Earth System Model
6	PMIP 3	MRI-CGCM3	Meteorological Research Institute
7	PMIP 4	EC-Earth3-Veg-LR	EC Earth Consortium
8	PMIP 4	MIROC-ES2L	Japan Agency for Marine-Earth Science and Technology
9	PMIP 4	MRI-ESM2-0	Meteorological Research Institute

source: Author (2021)

The comparison made was based on measures from Information Theory and Empirical Mode Decomposition and had the propose of assessing seasonality and variation modes aspects of the series. In order to rank the models, a multi-criteria decision analysis took place using the Technique for Order of Preference by Similarity to Ideal Solution (TOPSIS) algorithm as described in Hwang & Yoon (1981). Figure 1 illustrates the proposed comparison method, which starts with the series decomposition in seasonal components and pluriannual components. These components were compared to the observed series through the KL Divergence and Information Variation. After that, these measures served as input to the TOPSIS algorithm to rank the models in three scenarios.

Figure 1 - Model Comparison Methodology

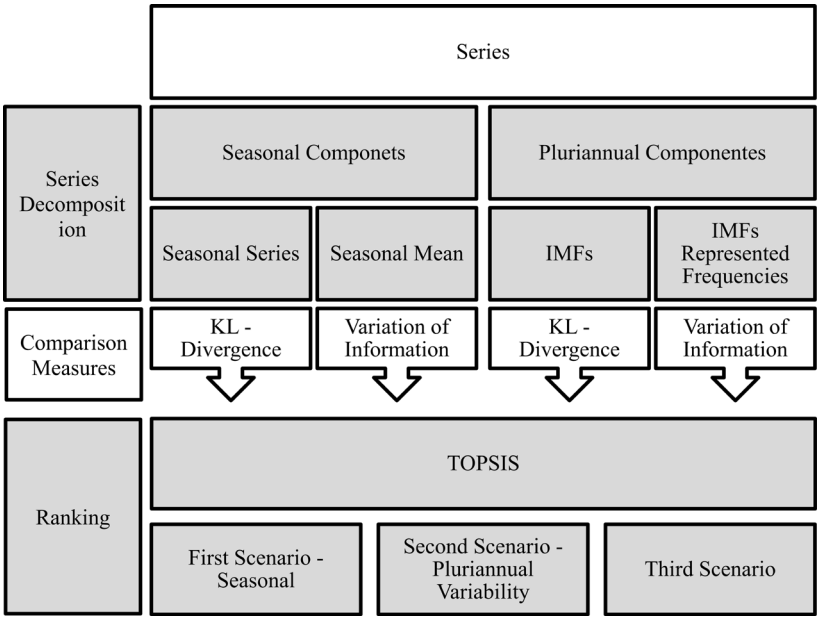

source: Author (2021)

In the second part, the top three models in the pluriannual variability scenario were analyzed to detect change point and variation modes in decadal and centennial scales. Additionally, models were compared against each other and to external forcings series to assess synchrony and patterns that could indicate if the oscillatory mode is due to internal variability or to external forcing. Figure 2 illustrates the adopted method for each part of the analysis, which consisted of Distribution Free CUSUM test for the change point detection, wavelet decomposition to assess variation modes and cross-wavelet spectra to assess synchrony.

Figure 2 - Series Pluriannual Assessment

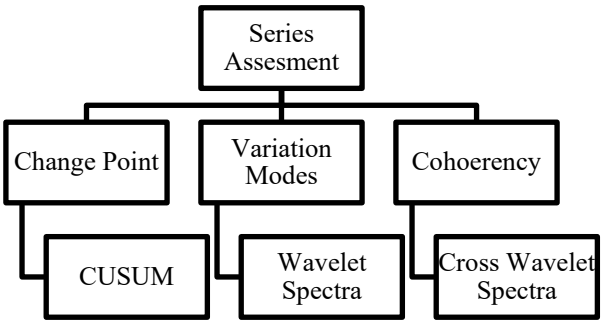

source: Author (2021)

3.2.2 Information Theory Measures

Claude Shannon's work published in 1948, entitled "A Mathematical Theory of Communication", laid the foundations for the field known today as Information Theory. Aiming to model communication through noisy channels and to take advantage of the statistical structure of the message to optimize channel capacity, Shannon developed the concept of entropy which proved to be useful in many scientific fields such as Economics, Cryptography, Informatics, and Statistics (Rioul, 2018)

Among the key concepts in information theory are information content, entropy, mutual information and variation of information. The information content concerns how much information a specific result of a random variable delivers, which could also be understood as the degree of surprise on learning that specific result, expressed by (1). Connected to this concept is Shannon Entropy which measures the average information delivered by a random variable, given its probability space, expressed by (2) for discrete random variables and by (3) for continuous one (Bishop, 2006).

$$h(x) = -\log p\,(x) \tag{1}$$

$$H(X) = -\sum p(x) log\ p(x) \tag{2}$$

$$H(X) = -\int p(x) log\ p(x) dx \tag{3}$$

The concept of entropy can be also extended to the joint entropy of two variables, simply by substituting regular probabilities by joint probabilities in (2) and (3) to obtain (4). Similarly, one can calculate the conditional entropy, that measures the uncertainty left in one variable given that we know the value of another variable. The expression of conditional entropy is obtained simply by substituting regular probabilities by conditional probabilities in

(2) and (3), as stated in (5) for a specific value of Y or in (6) for the actual conditional entropy (Cover & Thomas, 2006).

$$H(X,Y) = -\int p(x,y) log\ p(x,y) dx \tag{4}$$

$$H(X|Y=y) = -\int p(x|Y=y) log\ p(x|Y=y) dx \tag{5}$$

$$H(X|Y) = -\int p(x,y) log\ p(x|y) dx \tag{6}$$

Relative Entropy, or the KL Divergence, measures the additional information required to describe a random variable when probability distribution is misspecified, expressed by (7). In statistics, it is the expected log-likelihood ratio between two probability distributions, meaning that it measures the deviation between two probability distributions (Cover & Thomas, 2006).

$$\begin{aligned} KL(p \parallel q) &= -\int p(x) log q(x) dx - (-\int p(x) \log p(x) dx) \\ &= -\int p(x) log \frac{q(x)}{p(x)} dx \end{aligned} \tag{7}$$

Mutual Information, on the other hand, measures how much information the result of one variable conveys about another random variable. As expected, the concepts of mutual information and entropy are closely related. The mutual information of X and Y is the uncertainty of X minus the uncertainty of X after knowing the value of Y, as in (8). From (8), we could derive (9), since there is no uncertainty left when we know the variable's value. Figure 3 summarizes the relations between entropy and mutual information for variables X and Y (Cover & Thomas, 2006).

$$I(X,Y) = H(X) - H(X|Y) \tag{8}$$

$$I(X,X) = H(X) - H(X|X) = H(X) \tag{9}$$

Figure 3 - Entropy and Mutual Information Relationship

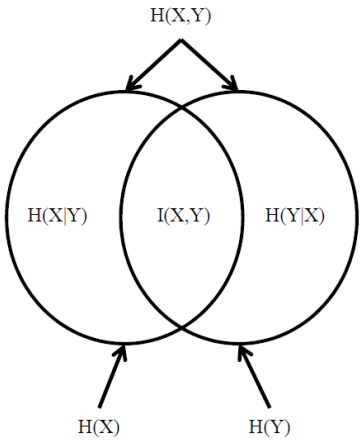

source: Cover & Thomas (2006)

Although mutual information is a useful measure, it is not a metric distance since expression (8) is different from zero. From Figure 1, one can derive a similarity measure called the Variation of Information (VI), which is a metric distance that expresses the similarity between two random variables. Note, in Figure 3, that mutual information would raise if the random variables are closely related while both the relative entropy would be small. Variation of Information is the sum of both relative entropy in Figure 1, given by (10) (Meilă, 2007).

$$VI(X,Y) = H(X|Y) + H(Y|X) = H(X) + H(Y) - 2I(X,Y) \tag{10}$$

As an application of Information Theory to model comparison, Correa & Lindstrom (2012) proposed a two-dimensional diagram, which takes advantage of the metric properties of the VI, denominated Mutual Information Diagram (MD). The MD is analog to Taylor Diagram (Taylor, 2001) but based on the relations between information theory measures. The diagram represents the models in a polar coordinate system with the radius given by the model´s entropy and the angle given by the cosine arc of a quantity c_{xy}, expressed in (11). In a diagram structured this way, the distance between two points is the VI, meaning that similar models will be close to each other, as illustrated in Figure 4.

$$c_{XY} = 2I(X,Y)\frac{H(X,Y)}{H(X)H(Y)} - 1 \tag{11}$$

Figure 4 - Mutual Information Diagram

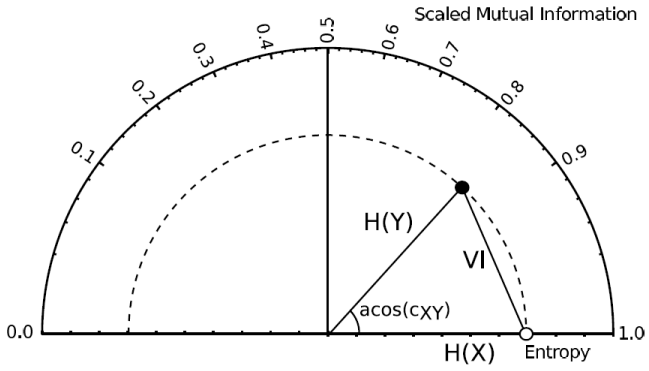

source: Correa & Lindstrom (2012)

The Mutual Information diagram is a simple way to summarize all measures about a set of models and also compare these models in a single picture. Additionally, it has the advantage of detecting any kind of dependency, even nonlinear, given that Mutual Information, unlike Pearson's correlation, it is not limited to linear dependency (Correa & Lindstrom, 2012).

3.2.3 Empirical Mode Decomposition

Empirical Mode Decomposition (EMD) was proposed by Huang et al. (1998) as a signal decomposition method. The EMD decomposes the signal into functions called the Intrinsic Mode Functions (IMF) through the sifting process. The IMF is, by construction, a locally symmetric function concerning the time axis, meaning that it satisfies two conditions: at any point, the mean value of the envelope is zero and the number of extreme points differs from the zero crossings at most by one.

The sifting process starts with drawing two envelopes, one connecting the maximum points, and another one connecting the minimum points. Then, the local average on these two envelopes is taken and subtracted from the original signal. This results in the first IMF which is then subtracted from the original signal before the same process is repeated to extract the second IMF. The sifting process is repeated until either the residue or the component reaches a predetermined small value. IMFs built this way represents oscillation modes extracted directly from the data, starting from the higher frequency mode in the first IMF to the lowest one in the last IMF. This contrasts with Wavelet analysis since wavelet basis are predetermined and the IMFs are extracted from the data (Huang et al., 1998).

Further improvement in the EMD was purposed by Wu & Huang (2009) and Torres et al. (2011), called the Ensemble EMD (EEMD) and the Complete Ensemble EMD (CEEMD). The EEMD generates new signals by adding white noise to the original one,

applies EMD independently to each new signal, and then takes the average IMF obtained for each mode as a result. This way, it was possible to avoid mode mixing and aliasing, which could prevent the IMF to have physical meaning. The CEEMD, on the other hand, takes the same procedure to obtain the first IMF but, for the second one, it starts by removing the average IMF calculated for the first mode from the signal and then applies the same method used to calculate the first mode IMF. This way, the CEEMD procedure guarantees that there will be no residual noise in the signal reconstruction and showed better spectral separation.

3.2.4 Technique for Order of Preference by Similarity to Ideal Solution - TOPSIS

TOPSIS algorithm is a method for multi-criteria decision making based on the Euclidean distance between the alternatives and both best possible alternative and worst possible alternative. The algorithm starts with a decision matrix in which rows refer to alternatives and columns to criteria, then the decision matrix columns are normalized and weighted. After that, the best possible alternative is determined considering the best attribute among the alternatives, and the worst possible solution is determined similarly. The Euclidian distance between each alternative and the best and worst possible solution is calculated to compose a relative closeness index to the best possible solution ranging from 0 to 1, where 0 means that the alternative is the worst possible alternative and 1 means that the alternative is the best possible alternative (Hwang & Yoon, 1981).

3.2.5 Model Selection

In order to define the comparison criteria, series were decomposed into seasonal components and pluriannual components, as in Figure 5. Seasonal components are composed by monthly rainfall organized in 12 series, one for each month in the year, and by the monthly seasonal means. The former was compared to the gauged series using the KL-Divergence as a measure, while the latter was compared using the VI. In the case of pluriannual components, the total annual rainfall series were decomposed into IMF´s, which were compared to gauged series in two ways. First, each IMF was compared to the gauged series IMF using KL-Divergence as a measure, then the average wavelet power spectrum was calculated for each IMF as described in Torrence & Compo (1998) and extracted only the portion with significant frequencies, which were compared to the gauged series using the VI.

The weight distribution for each measure in the TOPSIS algorithm followed three scenarios: the first one where only seasonal components were taken into account, the second one where only pluriannual components were considered, and the third one where seasonal

components shared half of the weight and the other half was shared between pluriannual components. In each scenario, 1000 simulations were made, where the weight distribution inside the seasonal components and the pluriannual components were randomly assigned. In the seasonal components, the weight for the seasonal mean was assigned through a uniform random variable, from 0 to 1. A portion of the remaining weight, calculated through a uniform random variable from 0.5 to 1, was shared between the months from January to June and the remaining portion to months from July to December. In the pluriannual components, part of the weight, calculated as a uniform random variable from 0.6 to 1, was shared between low-frequency IMF, comprising IMF 3 to 5, and the remaining was divided between IMF 1 and 2. Each IMF gave rise to two measures, a VI related to the frequencies represented in the IMF and a divergence to the gauged series IMF. These two measures had the same weight in the algorithm.

Figure 5 - Series decomposition

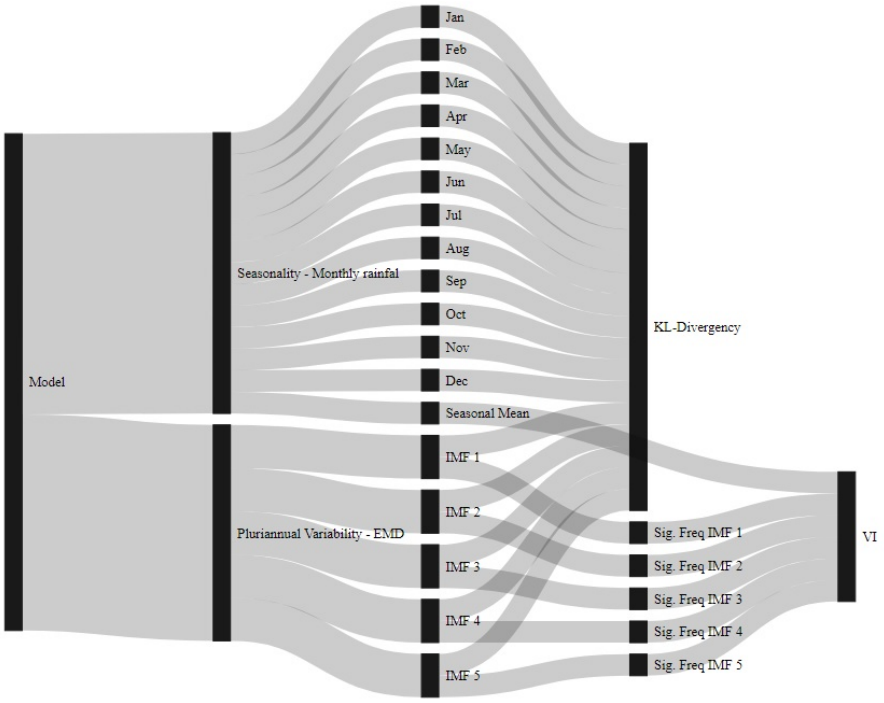

source: Author (2021)

3.2.6 Distribution Free CUSUM Test - CUSUM

The Distribution Free CUSUM Test is a change point detection method proposed by McGilchrist and Woodyer (1975) that doesn´t require any prior knowledge on the data probability distribution or the change point location. This test analyses the series deviation from the median by calculating the deviation for each value and applying the sign function.

The test statistics expressed in (12), where V_i is the cumulative sum of the sign function series given by (13), has the same distribution as Kolmogorov-Smirnov test statistics under the null hypothesis of no change in the distribution of the data. This way, for a chosen level of significance, there will be statistical evidence of change point if the cumulative sum series reaches the critical value.

$$\frac{1}{m} max(|V_i|) \tag{12}$$

$$V_i = \sum_{j=1}^{i} sign(x_i - k) \tag{13}$$

3.2.7 Spectral Analysis - Wavelet

Functions and signals spectral analysis had its starting point in the work of Fourier, who, in his study of heat conduction, decomposed a continuous and periodic function into a linear combination of sines and cosines (Vidakovic, 1999). Fourier´s analysis was successful in decomposing a signal in its various frequencies, but it is unable to deal with the signal´s variations over time. This limitation is related to the fact that sine and cosine functions have constant amplitude along the real line, so that it is not possible to locate the frequencies in the time domain (Ogden, 1997).

Several attempts were made to overcome this issue, among which Garbor´s Transform is highlighted. The main idea in this transform is to take a window, bounded by a function, to which the Fourier transform is applied. This way, since one can locate the window it is possible to locate frequencies in the time domain. There is, however, a shortcoming in this method which relates to the choice of the window size and the resolution tradeoff between frequency and time domain. If one selects a narrow window to obtain a better time resolution, then it is not possible to detect low frequencies. On the other hand, if one fixes a large window to detect lower frequencies, then the frequency location in time is prejudiced (Ogden, 1997).

In this context, wavelet analysis appears as a natural evolution on Fourier analysis, since one of its main properties is the compact support, which leads to the possibility of locating frequency in the time domain (Nason, 2008). The wavelet transform is obtained through a convolution operation between the signal and a scaled and translated version of the wavelet function, as in expression (14) for the case of discrete-time signal (Torrence & Compo, 1998).

$$W_n(s) = \sum_{n'=0}^{N-1} x_{n'}\, \psi^* \left[\frac{(n'-n)\delta t}{s}\right] \tag{14}$$

Wavelets are waveform functions that fulfill several requirements such as zero mean and compact support in both time and frequency domain (Torrence & Compo, 1998). Many functions are suited as wavelet, among which Nason (2008) mentions Haar, Daubechies, Shannon, Meyer and Coiflets wavelets, and Torrence & Compo (1998) mentions Morlet, Paul and DOG wavelets. In this study, the complex Morlet wavelet, given by expression (15), was adopted. The Morlet is a wave form function with a variable amplitude given by a gaussian function, hence it has a gaussian shape in frequency space, as illustrated in Figure 6.

$$\psi(t) = \pi^{-1/4} e^{iw_o t} e^{-t^2/2} \tag{15}$$

Figure 6 - Morlet Wavelet in the time domain (left) and in the frequency domain (right).

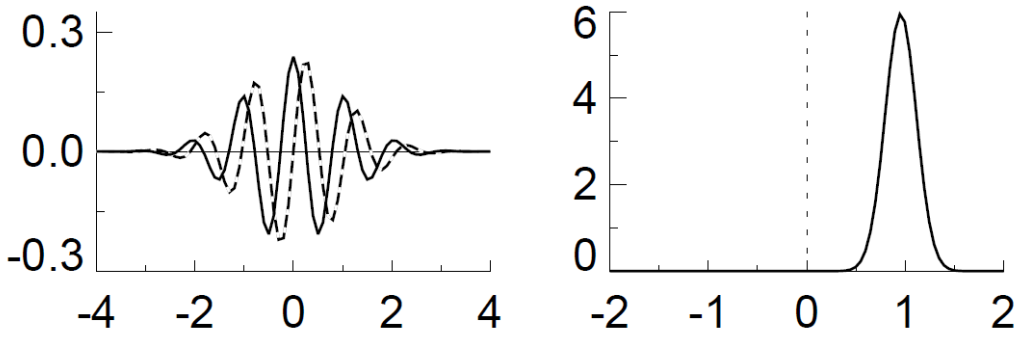

source: Torrence & Compo (1998)

Wavelet power is defined as the modulus of the wavelet transform and it can be assessed through the wavelet power spectrum, which is a graphical representation of the wavelet power through both time and frequency scale. The cross-wavelet power and the wavelet coherency spectrum are the tools to compare two signals and identify common oscillatory modes, which also allows to assess phase synchrony (Torrence & Compo, 1998). In this study, wavelet computations were done using *R* package *Waveletcomp.*

3.3 Results and Discussions

3.3.1 Model Selection

The VI criterion for seasonal mean is summarized in Figure 7 through the Mutual Information Diagram, where can be seen that bcc-csm1-1, CCSM4, and CSIRO-Mk3L-1-2 from PMIP 3 and MRI-ESM from PMIP4 are closer to the observed series, indicated as Funceme, meaning that seasonal means are better represented by these models. The VI for these series are 1,01, 0,91, 0,90 and 0,85 respectively. The models with the worst performance in this criterion are MPI-ESM-P and HadCM3 from PMIP3 and EC-Earth3 and MIROC from PMIP4, with VI of 2,00, 1,72, 1,57, and 1,47.

Figure 7 - Mutual Information Diagram for Seasonal Mean

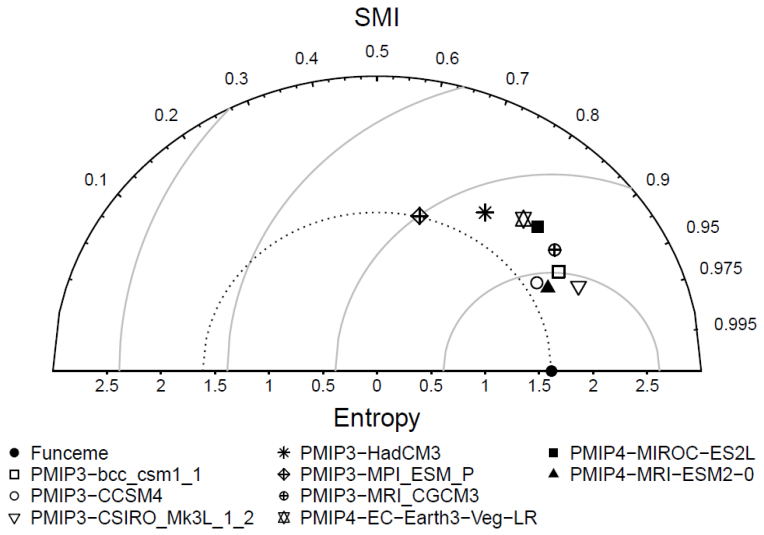

source: Author (2021)

The radar chart in Figure 8 shows the seasonal series divergence criterion summary, where each axis corresponds to a month and the value plotted corresponds to the divergence between the model and observe series for a specific month. The PMIP3 bcc-csm1-1 had the best performance for the wet period (January to June), followed by Hadcm3, MRI and CSIRO, all from PMIP3. For the dry period, PMIP3 Hadcm3 had the best performance, followed by PMIP3 CSIRO, PMIP4 MRI-ESM2 and PMIP4 MIROC-ES2L. In the overall performance, PMIP3 Hadcm3 was the closest to the observed series followed by CSIRO, bcc-csm1-1 and MIROC-ES2L, while the worst performance was from PMIP3 CCSM4, followed by PMIP4 EC-Earth3, PMIP3 MRI and PMIP3 MPI.

Additionally, one can note that although CCSM4 showed a good performance on the seasonal mean criterion it is not a good representation for the seasonal distribution. On the other way, PMIP3 Hadcm3 and MIROC-ES2L were among the worst models in representing the seasonal mean, but both had good adherence to the seasonal distribution.

Figure 8 - Seasonal Series KL- Divergence Radar Chart

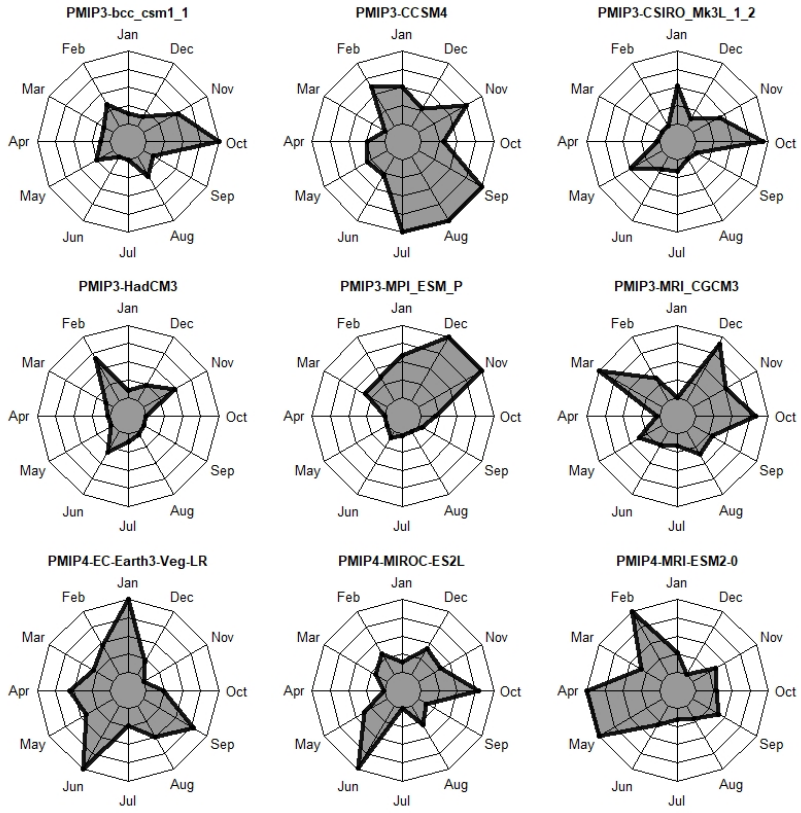

source: Author (2021)

The VI criterion for the IMFs average power spectra measures the adherence between the frequencies represented in Models IMFs to the ones represented in the observed series. This criterion was summarized in five Mutual Information Diagrams, one for each IMF. In the case of IMF 1, 2 and 3, illustrated in Figure 16 in APPENDIX, there was not much difference between the Models behavior. On the other hand, for the IMFs 4 and 5, both illustrated in Figure 9, it is possible to verify contrasting performances. The VI for IMF 4 shows best adherence in PMIP4 MIROC followed by PMIP3 HadCM3, while the poorest frequency representation was due to CSIRO and MRI, both from PMIP3. The remaining models had similar results, with VI ranging from 0,60 to 0,80. In the case of IMF 5, PMIP 4 EC Earth3 had the best performance, followed by PMIP3 HadCM3, while the models PMIP3 bcc-csm-1, PMIP3 CCSM4, PMIP4 MIROC and PMIP3 CSIRO had the worst representation. The remaining models had similar results, ranging from 1,10 to 1,50. In the overall

performance, considering IMFs 1 to 5, the models PMIP4 EC-Earth3 and PMIP3-HadCM3 had the best results, while the poorest performance was due to PMIP3 bcc-csm1-1 and PMIP3 CSIRO.

Figure 9 - Mutual Information Diagram for IMF´s Frequencies (IMFs 4 and 5)

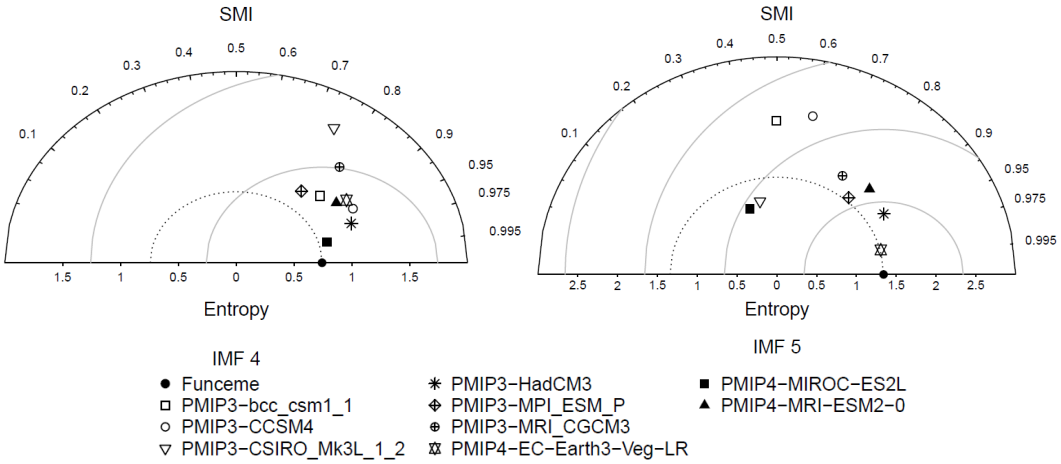

source: Author (2020)

The last criteria was the KL Divergence between series IMF and observed series, summarized in Figure 10 by a radar chart, in which each axis correspond to one IMF. Analyzing the high frequency, represented by IMFs 1 and 2, the best performance was achieved by PMIP3 MRI followed by PMIP3 HadCM3 and PMIP4 EC-Earth3, while the worst performance was due to PMIP4 MRI followed by PMIP3 CSIRO and PMIP3 MPI. On the lowest frequency spectra, represented by the remaining IMFs, PMIP3 HadCM3 had the best performance followed by PMIP4 EC-Earth3 and PMIP3 MPI, whereas PMIP3 CSIRO had the worst, followed by PMIP4 MIROC and PMIP3 CCSM4. In the overall performance, PMIP3 HadCM3 and PMIP4 EC-Earth3 also had the best results, while PMIP3 CSIRO PMIP4 MIROC showed the poorest results, which revealed that low frequency had the prevalent weight in this criterion. The results for this criterion was similar to the results for the VI criterion for the IMFs average power spectra, which achieved better results for PMIP4 EC-Earth3 and PMIP3-HadCM3.

Figure 10 - IMF KL-Divergence Radar Chart

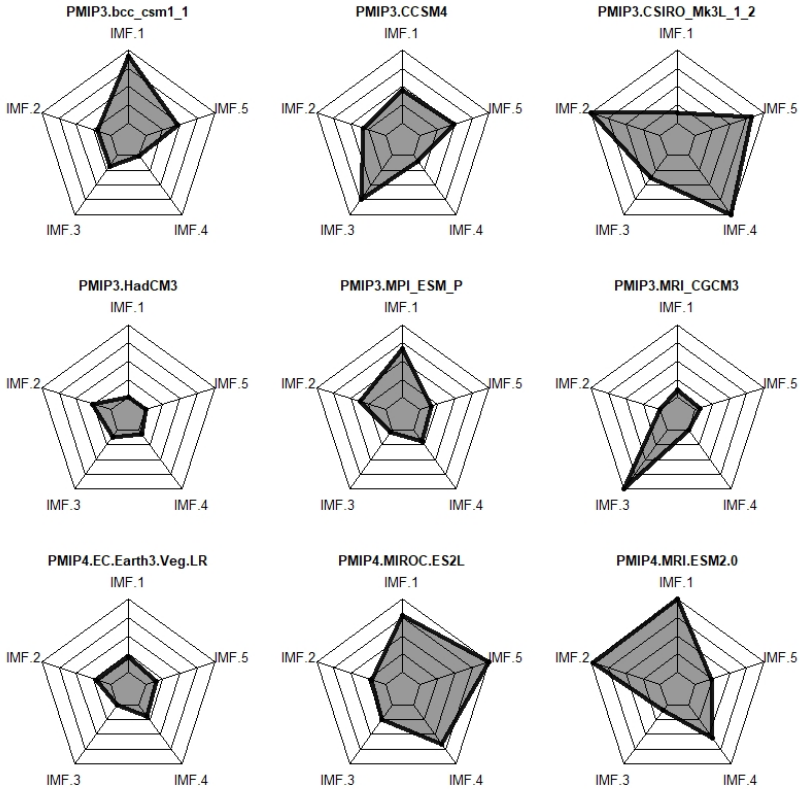

source: Author (2021)

The box-plot in Figure 11 illustrates TOPSIS Results for the simulations on the first scenario, which considers only seasonality. The chart shows that PMIP3 CSIRO, PMIP3 bcc-csm1-1 and PMIP3 CCSM4 are the models that better represent seasonality in NEB, while PMIP3 MPI, PMIP4 EC-Earth and PMIP3 HadCM3 had the worst representation among the studied models. These results show that the seasonal mean was prevalent, which was expected since this criterion has, on average, half the weight. It is also notable that Models that had contrasting performances in seasonality criteria tend to have higher score´s variance, as in PMIP4 MRI-ESM2 and PMIP3 HadCM3.

Figure 11 - TOPSIS Monte Carlo Simulation Results for the First Scenario

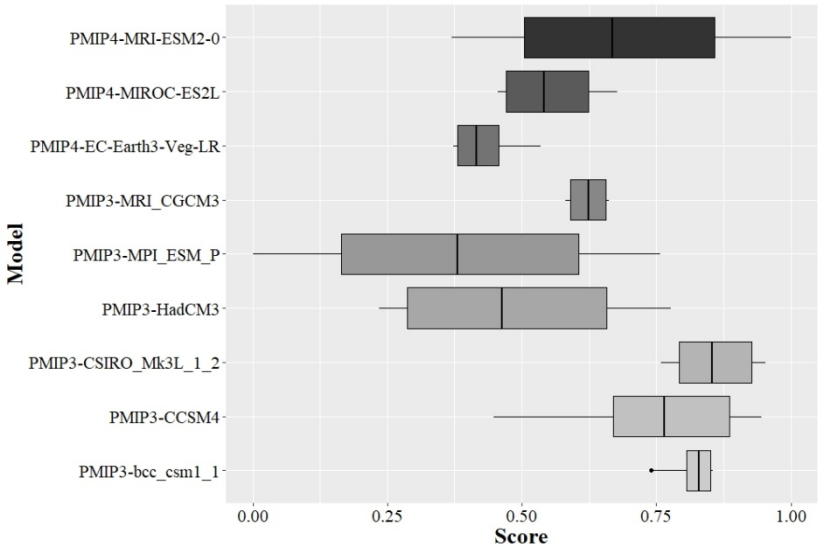

source: Author (2021)

The box-plot in Figure 12 displays the results for the second scenario, which considers only pluriannual variability. The score´s variance were lower in this scenario, which could be expected since the criteria adopted for pluriannual variability showed similar results for the models considered in this analysis. The PMIP3 HadCM3 achieved the best results, followed by PMIP3 MPI and PMIP4 EC-Earth3, whereas PMIP4 MIROC had the poorest result, followed by PMIP3 CSIRO and PMIP3 CGCM. Once again, results showed that the adherence in the lower frequency prevailed over the higher frequency in the analyzed models performance.

Figure 12 - TOPSIS Monte Carlo Simulation Results for the Second Scenario

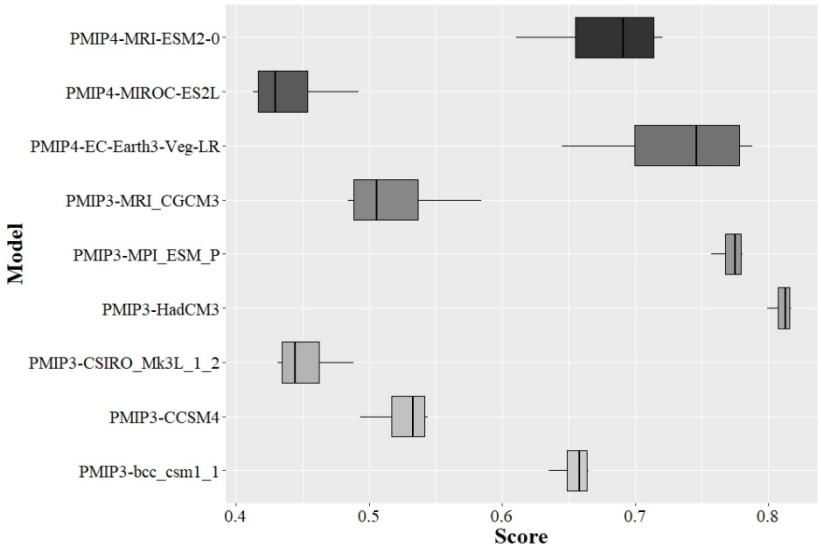

source: Author (2021)

The results for the third scenario are illustrated as a box-plot in Figure 13, where both seasonality and pluriannual variability criteria were considered with the same weight. The chart shows that PMIP3 bcc-csm1-1 achieved the best results, whereas PMIP4 MIROC which had the worst result. The remaining models had similar performance, with highlight to models with contrasting performances between seasonality and pluriannual variability such as HadCM3, PMIP3 MPI and PMIP4 EC-Earth3 which had good results for pluriannual variability and were among the worst results for seasonal criteria or PMIP3 CSIRO that had the best result for seasonal criteria and was among the worst results for pluriannual variability.

Figure 13 - TOPSIS Monte Carlo Simulation Results for the Third Scenario

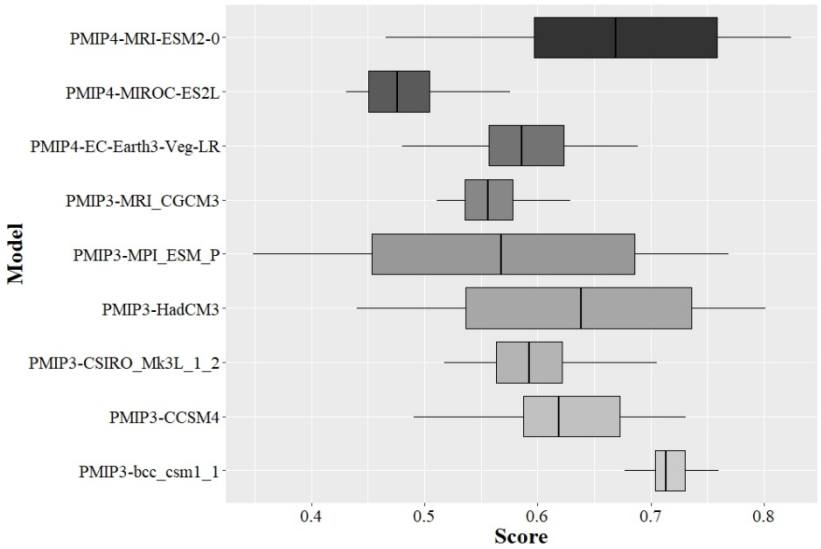

source: Author (2021)

The model´s rank, based on the average score obtained through Monte Carlo simulations, is summarized in Table 2 for each scenario assessed in this analysis. This way is possible to choose the model that best suits the analysis to be made, in this case, PMIP3 CSIRO should be the choice if the objective is to analyze seasonality and, if the aim is to analyze pluriannual variability, the choice should be PMIP3 HadCM3.

Table 2 - Models Rank

Rank	1st Scenario - Seasonality	2nd Scenario - Pluriannual Variability	3rd Scenario
1	CSIRO-Mk3L-1-2	HadCM3	bcc-csm1-1
2	bcc-csm1-1	MPI-ESM-P	MRI-ESM2-0
3	CCSM4	EC-Earth3-Veg-LR	HadCM3
4	MRI-ESM2-0	MRI-ESM2-0	CCSM4
5	MRI-CGCM3	bcc-csm1-1	CSIRO-Mk3L-1-2
6	MIROC-ES2L	CCSM4	EC-Earth3-Veg-LR
7	HadCM3	MRI-CGCM3	MPI-ESM-P
8	EC-Earth3-Veg-LR	CSIRO-Mk3L-1-2	MRI-CGCM3
9	MPI-ESM-P	MIROC-ES2L	MIROC-ES2L

source: Author (2021)

3.3.2 Last Millennium Change Point Detection

The distribution-free CUSUM test made no change point detection since none of the models CUSUM reached the critical value of 43 for 95% confidence. The CUSUM chart is in Figure 14 and also shows that all models are in a wet phase from 1300 to 1400 and in a dry phase from 1400 to 1450. Beyond that point, HadCM3 stays in a dry phase until 1600, while both MPI-ESM-P and EC-Earth3-Veg-LR are in a wet phase from 1450 to 1600. In the next period, from 1600 to 1700 all models are in a wet phase, whereas models are in a dry phase from 1700 to 1850, which was more pronounced in MPI-ESM-P and EC-Earth3-Veg-LR. The last period is consistent with historical records, which indicate at least three severe droughts: in the period from 1723 to 1729, in the period from 1777 to 1778, and in the year 1845 (Campos, 2014).

Figure 14 - CUSUM for the models: HadCM3 in red, MPI-ESM-P in green and EC-Earth3-Veg-LR in blue.

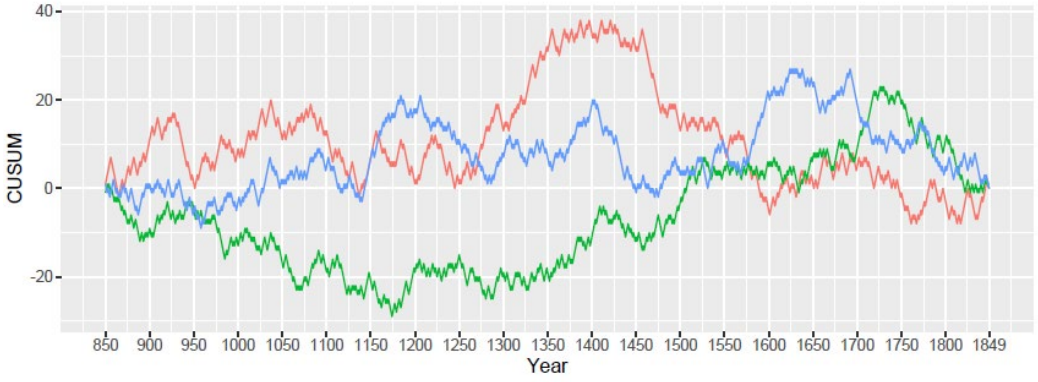

source: Author (2021)

3.3.3 Last Millennium Low Frequency Analysis

The wavelet power spectra and the average power diagram for the top three models are in Figure 15. The average wavelet power shows the significant signals in blue and red for significance levels of 10% and 5% respectively, which were shared by the three models in the period range of 4 to 8 years, 16 to 32 years, and 128 to 256 years. The first variation mode is consistent with El Niño-Southern Oscillation (ENSO) and was expected, given that Gregory Flato et al. (2018) reported that CMIP5 models were able to reproduce both ENSO and its tropical moist teleconnections. In the case of the second oscillation mode, with periods ranging from 16 to 32 years, the wavelet spectra show that there is no time synchrony between the models, while the last variation mode, with periods ranging from 128 to 256 years occurred almost at the same time for the three models, which raises the hypothesis that this oscillatory mode is externally forced. The Cross-Wavelet power spectra between the three models are in Figure 17 in APPENDIX, in which the phase difference is indicated by arrows, with horizontal right pointed arrow indicating that models are in phase and left pointed arrow indicating that models are out of phase. In the centennial oscillation mode there is a regular pattern with almost constant phase difference and smooth changes in dephasing, and there is also a phase alignment between the years 1300 and 1500.

Figure 15 - Wavelet Power Spectrum and Wavelet Average Power for the models a) HadCM3,b) MPI-ESM-P and c) EC-Earth3-Veg-LR.

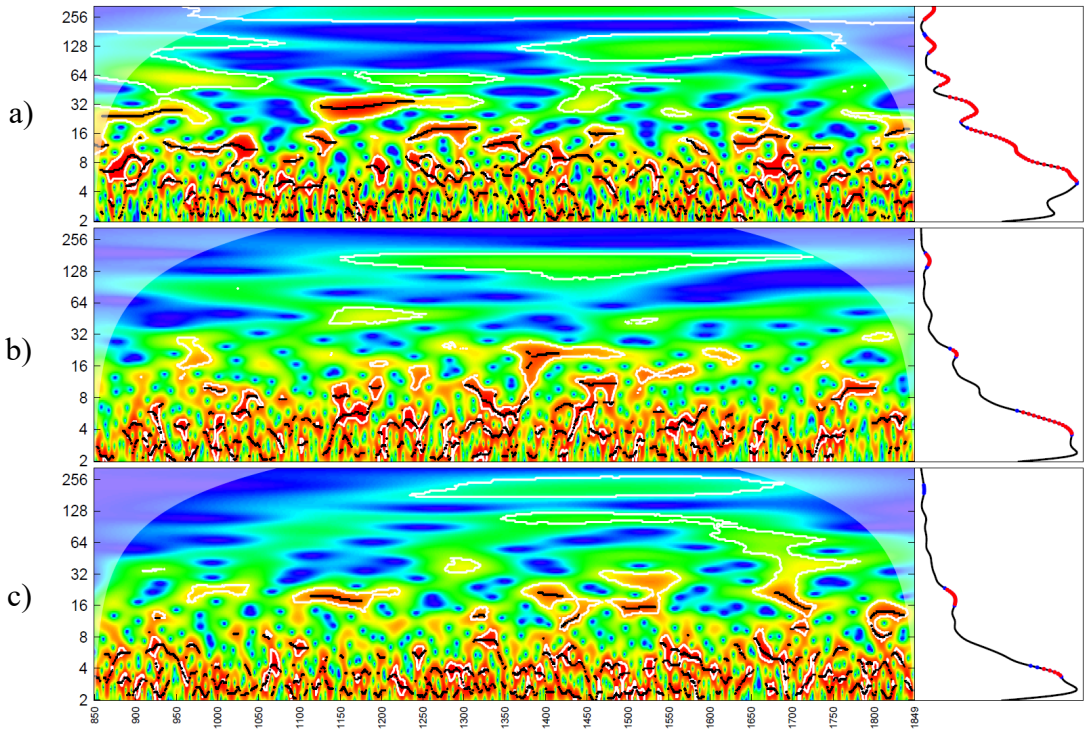

source: Author (2021)

The analysis turns to the solar forcing through the SATIRE-M Solar Forcing series. The series and wavelet power spectrum in Figure 18 shows that the solar forcing has strong oscillatory modes with periods ranging from 8 to 16 years and from 128 to 256 years. The latter oscillatory mode could be divided into two signals, one that is closer to 128 year period and is active during all the series, and a second one with a lower frequency that starts around the year 1150, reaches its peak in the year 1400 and stays active until the end of the period. The Cross-Wavelet Spectra between the SATIRE-M series and the models in Figure 19 in APPENDIX show a regular pattern for centennial modes phases, while no pattern was detected for the mode with periodicity between 16 and 32 years. In the case of volcanic forcing, Figure 20 in APPENDIX shows The Crowley data set for Volcanic Forcing and its wavelet power spectrum. Figure 20 also shows active oscillatory mode with periodicity between 128 and 256 years, with a stronger signal from the year 1200 onwards. Although there are active modes in other frequencies, the Cross-wavelet in Figure 21 shows that, for all series, the other modes are inactive during most of the period. On the centennial-scale however, the cross spectra show an active mode with periods ranging from 128 to 256 years during the entire period with a regular pattern in the phase difference between model and volcanic forcing. In summary, it seems that there is evidence that the oscillatory mode with periods ranging from 128 to 256 years could be caused by external forcing, while no evidence was found for the mode with periods ranging from 16 to 32 years.

3.4 Conclusion

This paper analyzed paleoclimatic model´s rainfall output, from PMIP´s last millennium experiment, aiming to assess the climate variability in its full range. In the first part, a model selection method based on measures from information theory was proposed. This method decomposes the historical output series in seasonal and pluriannual components and compares them to observed series components using Variation of Information and the KL-Divergence. Models were ranked through the TOPSIS multi-criteria decision algorithm, in three different scenarios: the first one considers only seasonal components, the second considers pluriannual components, while the third one considers both seasonal and pluriannual components. Simulations in the seasonality scenario showed that CSIRO-Mk3L-1-2, bcc-csm1-1, and CCSM4 were the models with the best adherence to the observed series, while simulations in the pluriannual scenario showed that HadCM3, MPI-ESM-P, and EC-Earth3-Veg-LR were the models with the best adherence. In the third scenario, the best performance was due to models bcc-csm1-1, MRI-ESM2-0, and HadCM3.

In the second part of the paper, the *past1000* experiment output for the top three models in the pluriannual scenario were analyzed in order to detect change point and oscillatory modes. Models were also compared to two of the major external forcing in other to assess whether the oscillatory modes were due to the external forcings or to the system´s internal variability. The distribution-free CUSUM test for change point detection made no change point detection in the series with a confidence level of 95%. The oscillatory modes were analyzed through wavelet decomposition and detected modes with a period range of 4 to 8 years, 16 to 32 years, and 128 to 256 years. The latter variation mode appeared to have time synchrony between the models and, beyond that, the cross-wavelet spectra showed a regular pattern in phase difference, with phase alignment in the period from the year 1300 to 1500. The analysis of solar irradiation and volcanic forcings, through wavelet power spectra, showed a strong signal in the oscillatory mode with a period range from 128 to 256, and the cross-wavelet spectra also showed a regular pattern in the phase difference between models and forcing series. Given these points, it seems that there is evidence that the oscillatory mode with a period ranging from 128 to 256 years could be caused by external forcings.

4 CONCLUSIONS

Rainfall variability patterns are key knowledge to water resources planning. However, inferring this variability is rather difficult given that observed rainfall series may not be representative of the full range of rainfall variability in current climatic conditions. Paleoclimatic proxy variables and paleoclimatic models emerged as possible solutions to assess the climatic variability through the reconstruction of the climate of the past, which provides longer series that may represent better the climate variability. This study assessed the rainfall variability in NEB through paleoclimatic models rainfall output for the PMIP´s LM experiment.

In the first part, the historical series for each model was compared to the observed series to evaluate the model´s capacity to represent the NEB´s climate. The adopted criteria were divided into seasonal and pluriannual components. Seasonal components analysis went beyond the usual seasonal means comparisons and also considered the adherence to the underlying probability distribution for seasonal series through the KL-Divergence. For pluriannual components, rainfall annual series were decomposed in IMF´s, which represent the embedded oscillatory modes, and were compared in two ways: adherence of the oscillatory modes represented in each IMF to historical series IMF and adherence to the underlying probability distribution through the KL-divergence. The series decomposition in both seasonal and pluriannual components associated with measures from Information Theory provided a deeper understanding of the model´s capabilities to represent the region´s climate.

Models were ranked from the measures computed for seasonal and pluriannual components with the TOPSIS algorithm, which considered three scenarios: seasonal components, pluriannual components, and both seasonal and pluriannual. The rank was determined from 1000 simulations for each scenario, with weights assignment varying accordingly to a random uniform distribution with a predetermined range. The ranking designed this way is robust to weights variation and the scenarios allow model selection to meet the analysis scope.

In the second part, the top three models ranked for the second scenario were analyzed to assess the low-frequency oscillatory modes. Variation modes with periods ranging from 4 to 8 years, 16 to 32 years, and 128 to 256 years were detected in all models. Cross-Wavelet power spectra showed time synchrony in the variation modes with period ranging from 128 to 256 years, which is evidence that this variation mode could be externally

forced. This evidence was supported by solar and volcanic forcing wavelet spectra and cross-wavelet between model series and external forcings.

It is recommended that future studies include metrics that consider the spatial patterns that could be coupled with the model evaluation method proposed in this study. Furthermore, it is recommended to assess the risk of pluriannual droughts considering the low-frequency patterns identified in this study.

REFERENCES

Almagro, A., Oliveira, P. T. S., Rosolem, R., Hagemann, S., & Nobre, C. A. (2020). Performance evaluation of Eta/HadGEM2-ES and Eta/MIROC5 precipitation simulations over Brazil. *Atmospheric Research*, *244*(May), 105053. https://doi.org/10.1016/j.atmosres.2020.105053

Bishop, C. M. (2006). *Pattern Recognition and Machine Learning*. New York, NY: Springer Science.

Braconnot, P., Harrison, S. P., Kageyama, M., Bartlein, P. J., Masson-Delmotte, V., Abe-Ouchi, A., … Zhao, Y. (2012). Evaluation of climate models using palaeoclimatic data. *Nature Climate Change*, *2*(6), 417–424. https://doi.org/10.1038/nclimate1456

Campos, J. N. B. (2014). Secas e políticas públicas no semiárido: Ideias, pensadores e períodos. *Estudos Avancados*, *28*(82), 65–88. https://doi.org/10.1590/S0103-40142014000300005

Campos, J. N. B. (2015). Paradigms and Public Policies on Drought in Northeast Brazil: A Historical Perspective. *Environmental Management*, *55*(5), 1052–1063. https://doi.org/10.1007/s00267-015-0444-x

Cook, E. R., Palmer, J. G., Ahmed, M., Woodhouse, C. A., Fenwick, P., Usama, M., … Khan, N. (2013). Five centuries of Upper Indus River flow from tree rings. *Journal of Hydrology*, *486*(August 2012), 365–375. https://doi.org/10.1016/j.jhydrol.2013.02.004

Correa, C. D., & Lindstrom, P. (2012). the Mutual Information Diagram for Uncertainty Visualization. *International Journal for Uncertainty Quantification*, *3*(3), 187–201. https://doi.org/10.1615/int.j.uncertaintyquantification.2012003959

Cover, T. M., & Thomas, J. A. (2006). *Elements of Information Theory* (2nd ed.). New Jersey, NY: John Wiley & Sons.

Dias, T. A., Costa, A. A., Sousa Filho, F. de A., & Silveira, C. da S. (2019). Análise das Simulações do PMIP3 Sobre o Nordeste Brasileiro Para o Período Pré-Industrial e Holoceno Médio. *Revista Brasileira de Meteorologia*, *34*(1), 109–119. https://doi.org/10.1590/0102-77863340023

Gomes, D. F., Albuquerque, A. L. S., Torgan, L. C., Turcq, B., & Sifeddine, A. (2014). Assessment of a diatom-based transfer function for the reconstruction of lake-level changes in Boqueirão Lake , Brazilian Nordeste. *Palaeogeography, Palaeoclimatology, Palaeoecology*, *415*, 105–116. https://doi.org/10.1016/j.palaeo.2014.07.009

Gregory Flato, Jochem Marotzke, Babatunde Abiodun, Pascale Braconnot, Sin Chan Chou, William Collins, Peter Cox, Fatima Driouech, Seita Emori, Veronika Eyring, Chris Forest, Peter Gleckler, Eric Guilyardi, Christian Jakob, Vladimir Kattsov, Chris Reason, M. R. (2018). Evaluation of climate models. In V. B. and P. M. M. Stocker, T.F., D. Qin, G.-K. Plattner, M. Tignor, S.K. Allen, J. Boschung, A. Nauels, Y. Xia (Ed.), *Climate Change 2013: The Physical Science Basis. Contribution of Working Group I to the Fifth Assessment Report of the Intergovernmental Panel on Climate Change [Stocker, T.F., D. Qin, G.-K. Plattner, M. Tignor, S.K. Allen, J. Boschung, A. Nauels, Y. Xia,* (p. 1858). Cambridge, United Kingdom and New York, NY, USA,: Cambridge University Press.

Huang, N. E., Shen, Z., Long, S. R., Wu, M. C., Snin, H. H., Zheng, Q., … Liu, H. H. (1998). The empirical mode decomposition and the Hubert spectrum for nonlinear and non-stationary time series analysis. *Proceedings of the Royal Society A: Mathematical, Physical and Engineering Sciences*, *454*(1971), 903–995. https://doi.org/10.1098/rspa.1998.0193

Hwang, C.-L., & Yoon, K. (1981). Multiple Attribute Decision Making Methods and Applications. In *Lecture Notes in Economics and Mathematical Systems* (1st ed., Vol. 618). Berlin: Springer-Verlag.

Jungclaus, J. H., Bard, E., Baroni, M., Braconnot, P., Cao, J., Chini, L. P., … Zorita, E. (2017). The PMIP4 contribution to CMIP6 - Part 3: The last millennium, scientific objective, and experimental design for the PMIP4 past1000 simulations. *Geoscientific Model Development*, *10*(11), 4005–4033. https://doi.org/10.5194/gmd-10-4005-2017

Kundzewicz, Z. W., Rosbjerg, D., Sevionovic, S. P., & Takeuchi, K. (1993). Extreme hydrological events in perspective. *Extreme Hydrological Events: Precipitation, Floods and Droughts (Proceedings of the Yokohama Symposium)*, (2), 1–8.

Malevich, S. B., Woodhouse, C. A., & Meko, D. M. (2013). Tree-ring reconstructed hydroclimate of the Upper Klamath basin. *Journal of Hydrology*, *495*, 13–22. https://doi.org/10.1016/j.jhydrol.2013.04.048

Mann, M. E., Steinman, B. A., Brouillette, D. J., & Miller, S. K. (2021). Multidecadal climate oscillations during the past millennium driven by volcanic forcing. *Science*, *371*(6533), 1014–1019. https://doi.org/10.1126/science.abc5810

Martin, J. T., Pederson, G. T., Woodhouse, C. A., Cook, E. R., Mccabe, G. J., Wise, E. K., … King, J. (2019). 1200 years of Upper Missouri River stream fl ow reconstructed from tree rings. *Quaternary Science Reviews*, *224*, 105971. https://doi.org/10.1016/j.quascirev.2019.105971

Martins, E. S. P. R., & Magalhães, A. R. (2015). A seca de 2012-2015 no Nordeste e seus impactos. *Parcerias Estratégicas*, *20*(41), 107–128.

Masson-Delmotte, V., M. Schulz, A. Abe-Ouchi, J. Beer, A. Ganopolski, J.F. González Rouco, E. Jansen, K. Lambeck, J. Luterbacher, T. Naish, T. Osborn, B. Otto-Bliesner, T. Quinn, R. Ramesh, M. Rojas, X. S. and A. T. (2013). Information from paleoclimate archives. In V. B. and P. M. M. Stocker, T.F., D. Qin, G.-K. Plattner, M. Tignor, S.K. Allen, J. Boschung, A. Nauels, Y. Xia (Ed.), *Climate Change 2013 the Physical Science Basis: Working Group I Contribution to the Fifth Assessment Report of the Intergovernmental Panel on Climate Change* (Vol. 9781107057, pp. 383–464). https://doi.org/10.1017/CBO9781107415324.013

McGilchrist, C. A., & Woodyer, K. D. (1975). Note on a Distribution-free CUSUM Technique. *Technometrics*, *17*(3), 321–325.

Meilă, M. (2007). Comparing clusterings-an information based distance. *Journal of Multivariate Analysis*, *98*(5), 873–895. https://doi.org/10.1016/j.jmva.2006.11.013

Miller, K. A., Hamlet, A. F., & Kenney, D. . (2018). Introduction: the context for western water policy and planning. In *Water Policy and Planning in a Variable and Changing*

Climate. (pp. 3–15). Boca Raton, FL: CRC Press.

Milly, P. C. D., Betancourt, J., Falkenmark, M., Hirsch, R. M., Zbigniew, W., Lettenmaier, D. P., & Stouffer, R. J. (2008). *Stationarity Is Dead: Whither Water Management?* (February), 573–574.

Nason, G. P. (2008). *Wavelet Methods in Statistics with R*. New York, NY: Springer.

National Academies of Sciences and Medicine, E. (2016). *Frontiers in Decadal Climate Variability: Proceedings of a Workshop* (A. Purcell & N. Huddleston, eds.). https://doi.org/10.17226/23552

Ogden, R. T. (1997). *Essential Wavelets for Statistical Applications and Data Analysis*. Cambridge-MA: Birkhäuser Boston.

Rioul, O. (2018). *Teoria da Informação e da Codificação*. Campinas, SP: Editora da Unicamp.

Roberto, J., Aragão, V., Groenendijk, P., & Sergio, C. (2019). Dendrochronologia Dendrochronological potential of four neotropical dry-forest tree species : Climate-growth correlations in northeast Brazil. *Dendrochronologia*, *53*(October 2018), 5–16. https://doi.org/10.1016/j.dendro.2018.10.011

Samadi, S. Z., Sagareswar, G., & Tajiki, M. (2010). Comparison of General Circulation Models: methodology for selecting the best GCM in Kermanshah Synoptic Station, Iran. *International Journal of Global Warming*, *2*(4), 347–365. https://doi.org/10.1504/IJGW.2010.037590

Schmidt, G. A., Jungclaus, J. H., Ammann, C. M., Bard, E., Braconnot, P., Crowley, T. J., … Vieira, L. E. A. (2011). Climate forcing reconstructions for use in PMIP simulations of the last millennium (v1.0). *Geoscientific Model Development*, *4*(1), 33–45. https://doi.org/10.5194/gmd-4-33-2011

Schmidt, G. A., Jungclaus, J. H., Ammann, C. M., Bard, E., Braconnot, P., Crowley, T. J., … Vieira, L. E. A. (2012). Climate forcing reconstructions for use in PMIP simulations of the Last Millennium (v1.1). *Geoscientific Model Development*, *5*(1), 185–191. https://doi.org/10.5194/gmd-5-185-2012

Taylor, K. E. (2001). Summarizing multiple aspects of model performance in a single diagram. *Journal of Geophysical Research Atmospheres*, *106*(D7), 7183–7192. https://doi.org/10.1029/2000JD900719

Taylor, K. E., Stouffer, R. J., & Meehl, G. A. (2012). An overview of CMIP5 and the experiment design. *Bulletin of the American Meteorological Society*, *93*(4), 485–498. https://doi.org/10.1175/BAMS-D-11-00094.1

Thorarinsdottir, T. L., Gneiting, T., & Gissibl, N. (2013). Using Proper Divergence Functions to Evaluate Climate Models. *SIAM/ASA Journal on Uncertainty Quantification*, *1*(1), 522–534. https://doi.org/10.1137/130907550

Torrence, C. (University of C., & Compo, G. P. (University of C. (1998). A Practical Guide to Wavelet Analysis. *Bulletin of the American Meteorological Society*, *79*(1), 61–78.

Torres, M. E., Colominas, M. A., Schlotthauer, G., & Flandrin, P. (2011). A complete ensemble empirical mode decomposition with adaptive noise. *ICASSP, IEEE International Conference on Acoustics, Speech and Signal Processing - Proceedings*, (May 2014), 4144–4147. https://doi.org/10.1109/ICASSP.2011.5947265

Viana, J. C. C., Sifeddine, A., Turcq, B., Albuquerque, A. L. S., Moreira, L. S., Gomes, D. F., & Cordeiro, R. C. (2014). A late Holocene paleoclimate reconstruction from Boqueirão Lake sediments, northeastern Brazil. *Palaeogeography, Palaeoclimatology, Palaeoecology*, *415*, 117–126. https://doi.org/10.1016/j.palaeo.2014.07.010

Vidakovic, B. (1999). *Statistical Modeling by Wavelets*. New York, NY: John Wiley & Sons.

Wallace, J. M., & Hobbs, P. V. (2006). Atmospheric Science: An Introductory Survey. In *Atmospheric Science: An Introductory Survey: Second Edition*. https://doi.org/10.1016/C2009-0-00034-8

Wils, T. H. G., Eshetu, Z., Bra, A., Gebrekirstos, A., Couralet, C., Robertson, I., … Beeckman, H. (2010). *Dendrochronology in the dry tropics : the Ethiopian case*. https://doi.org/10.1007/s00468-010-0521-y

Woodhouse, C.A., J.J., L., Morino, K., Meko, D. M., & Hirschboeck, K. K. (2016). Using the Past to Plan for the Future - The Value of Paleoclimate Reconstructions for Water Resource Planning. In K. A. Miller, A. F. Hamlet, D. S. Kenney, & K. T. Redmond (Eds.), *Water Policy and Planning in a Variable and Changing Climate* (pp. 161–182). Boca Raton, FL: CRC Press.

Woodhouse, Connie A., & Overpeck, J. T. (1998). 2000 Years of Drought Variability in the Central United States. *Bulletin of the American Meteorological Society*, *79*(12), 2693–2714. https://doi.org/10.1175/1520-0477(1998)079<2693:YODVIT>2.0.CO;2

Woodhouse, Connie A, Pederson, G. T., & Gray, S. T. (2011). An 1800-yr record of decadal-scale hydroclimatic variability in the upper Arkansas River basin from bristlecone pine. *Quaternary Research*, *75*(3), 483–490. https://doi.org/10.1016/j.yqres.2010.12.007

Worbes, M., & Nin, E. (2002). *One hundred years of tree-ring research in the tropics ± a brief history and an outlook to future challenges*. *2*, 217–231.

Worku, G., Teferi, E., Bantider, A., Dile, Y. T., & Taye, M. T. (2018). Evaluation of regional climate models performance in simulating rainfall climatology of Jemma sub-basin, Upper Blue Nile Basin, Ethiopia. *Dynamics of Atmospheres and Oceans*, *83*(October 2017), 53–63. https://doi.org/10.1016/j.dynatmoce.2018.06.002

World Meteorological Organization. (2006). Drought monitoring and early warning : concepts , progress and future challenges. In *World Meteorogical Organization*. Retrieved from http://www.wamis.org/agm/pubs/brochures/WMO1006e.pdf

Wu, Z., & Huang, N. E. (2009). Ensemble Empirical Mode Decomposition: A Noise-Assisted Data Analysis Method. *Advances in Adaptive Data Analysis*, *1*(1), 1–41. https://doi.org/10.1142/S1793536909000047

APPENDIX

Figure 16 - Mutual Information Diagram for IMF´s Frequencies (IMFs 1, 2 and 3)

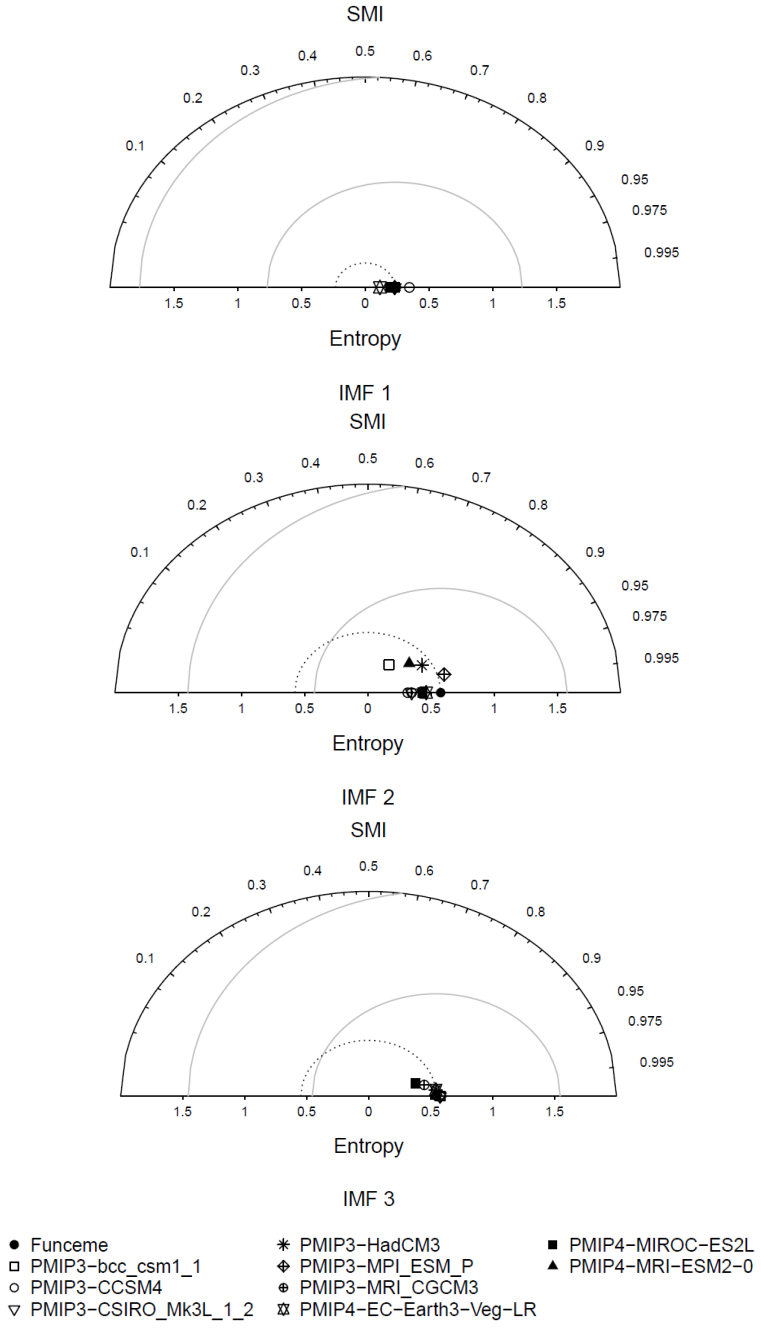

source: Author (2021)

Figure 17 - Cross-Wavelet Power Spectrum a) HadCM3 and MPI-ESM-P, b) HadCM3 and EC-Earth3-Veg-LR, and c) MPI-ESM-P and EC-Earth3-Veg-LR.

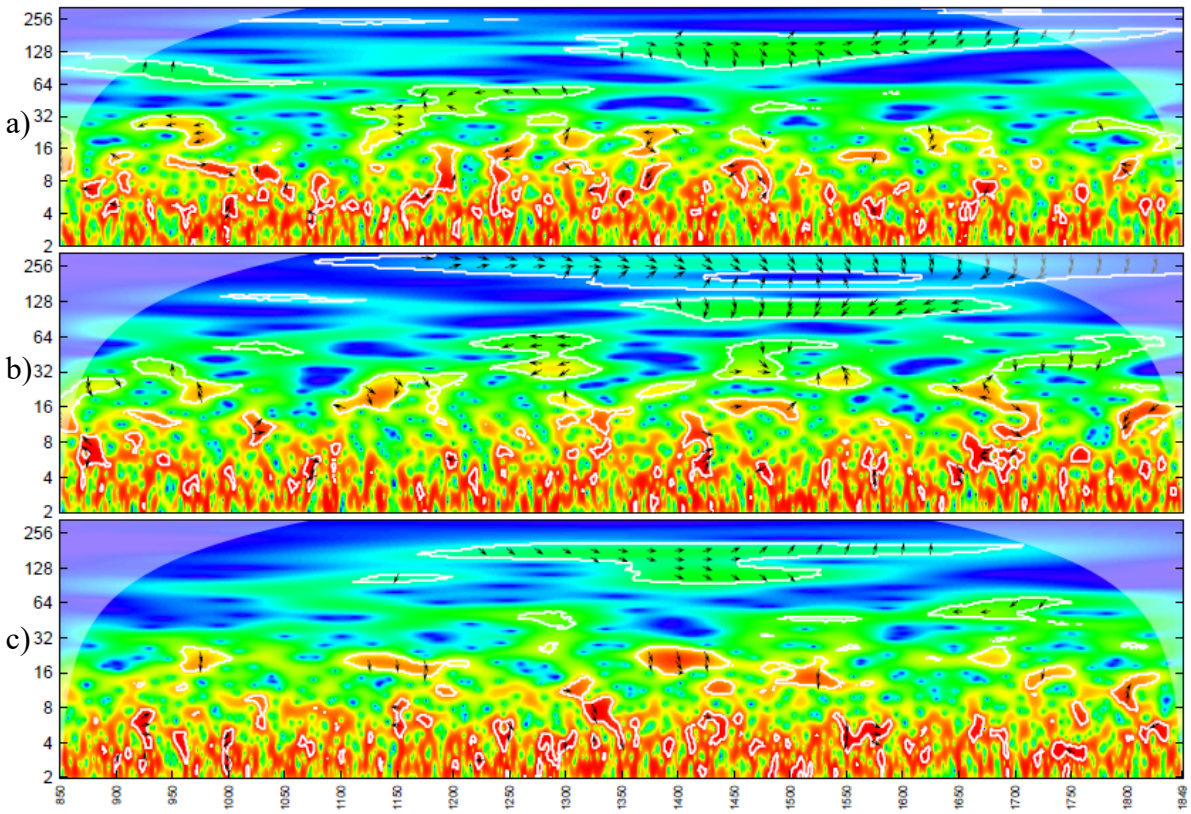

source: Author (2021)

Figure 18 - PMIP4 SATIRE-M Solar Forcing Series and the Solar Forcing Wavelet Power Spectrum

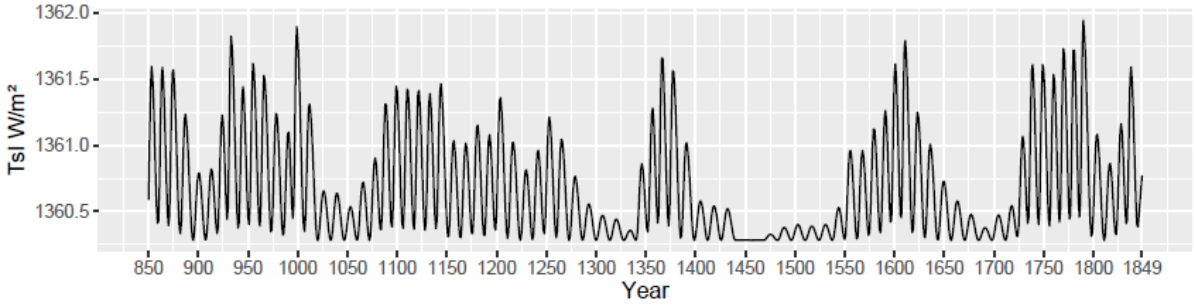

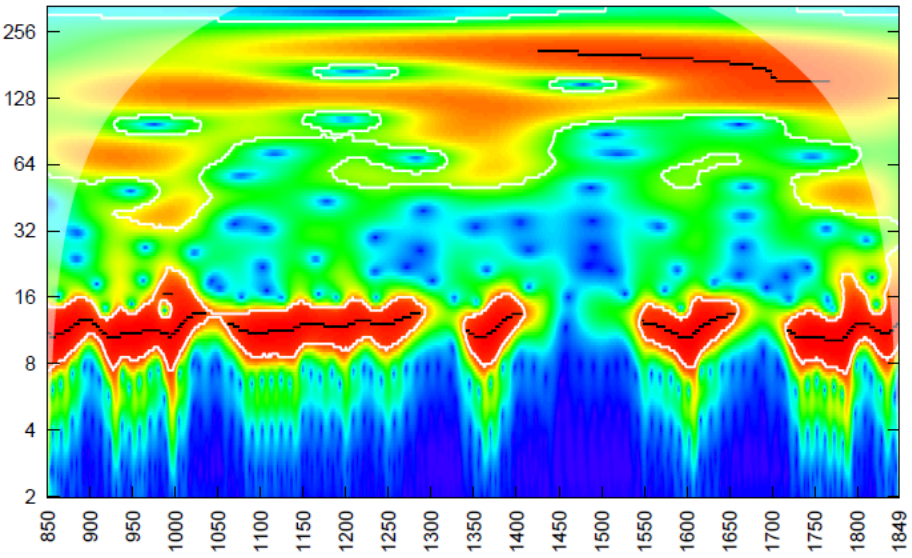

source: Author (2021)

Figure 19 - Cross-Wavelet Spectra: a) TSI and HadCM3, b) TSI and MPI-ESM-P and c) TSI and EC-Earth3-Veg-LR

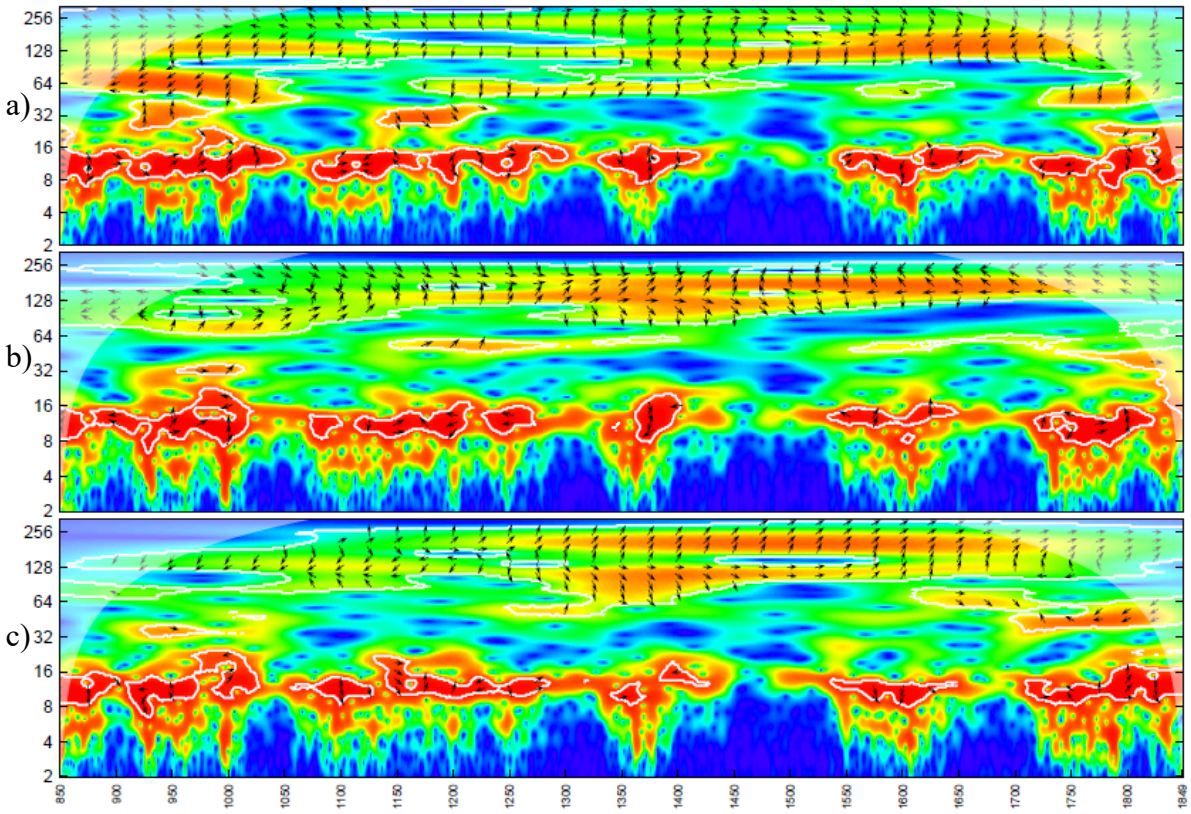

source: Author (2021)

Figure 20 - The Crowley data set for Volcanic Forcing - Series and Wavelet Power Spectrum

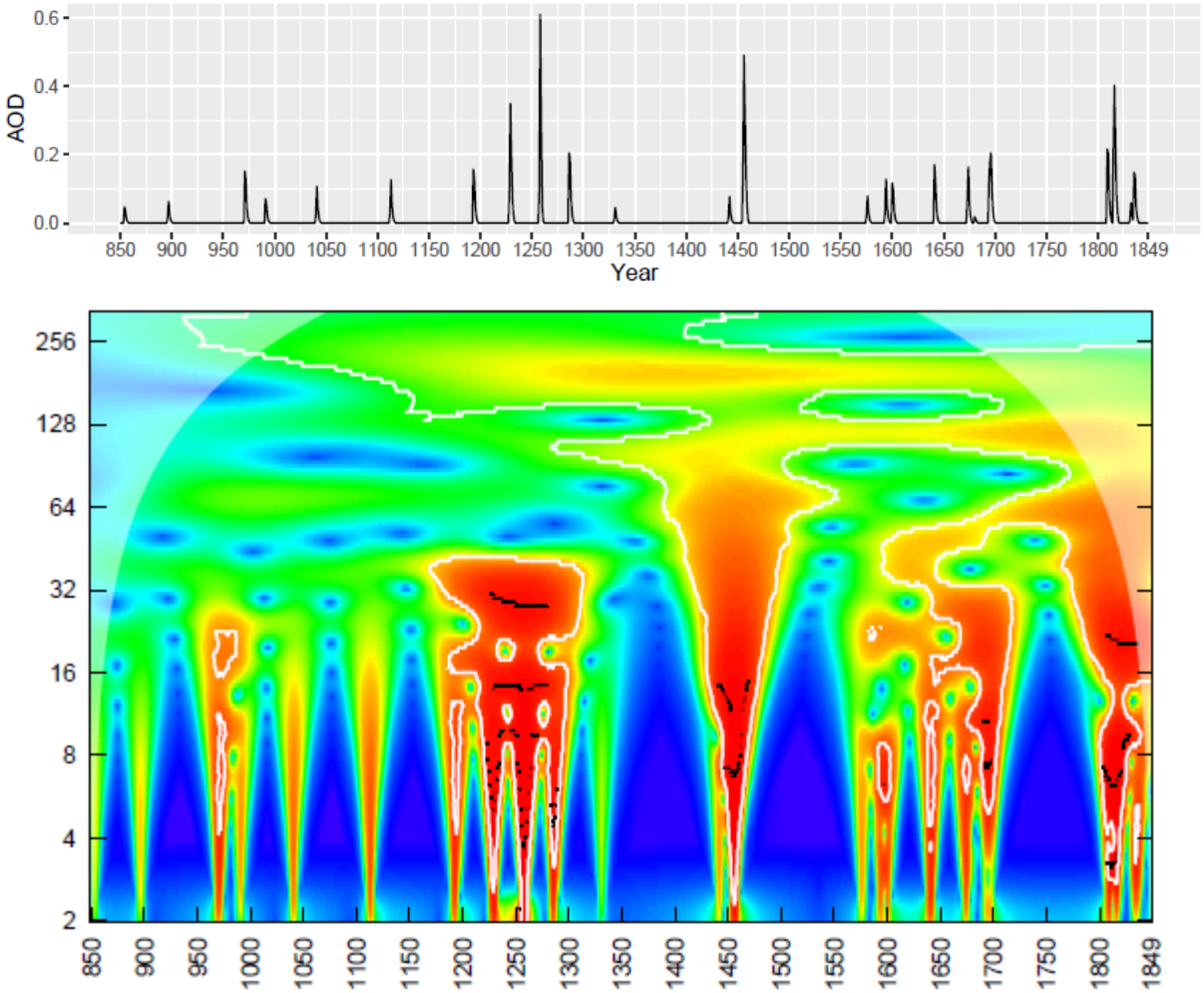

source: Author (2021)

Figure 21 - Cross-Wavelet Spectra: a) AOD and HadCM3, b) AOD and MPI-ESM-P and c) AOD and EC-Earth3-Veg-LR

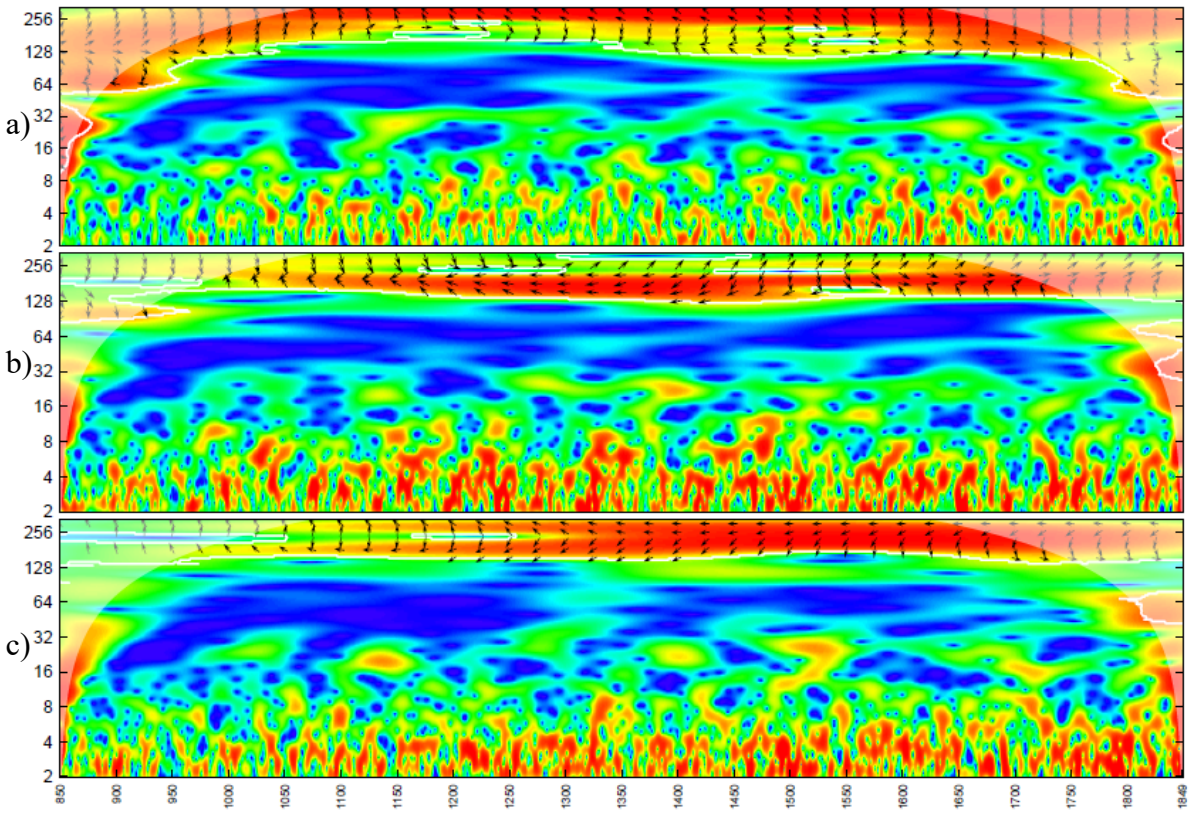

source: Author (2021)